TÉCNICO LISBOA

May 2023

The role of the flanking polyQ regions of Huntingtin exon 1 on lipid binding: Insights into Huntington's disease

Gonçalo Filipe Ferreira Damas

Abstract

Huntington's disease (HD) is a severe, autosomal dominant and progressive neurodegenerative disorder. HD is caused by a polyglutamine (polyQ) expansion within the first exon of the huntingtin (HTT) protein. The HTT exon 1 (Httex1) fragment with a polyQ expansion is highly toxic and forms aggregates/inclusion bodies in neural cells, replicating much of HD's pathology. Biological membranes play a critical role in Httex1 aggregation and toxicity. In this work, the interaction of Httex1-23Q with large unilamellar vesicles (LUVs) of different lipid compositions (with pure zwitterionic lipids, raft-mimicking mixtures and anionic lipids) was analyzed by Acrylodan and Atto 488 fluorescence. Each flanking polyQ region – N-terminal Nt17 and C-terminal proline-rich region (PPR) – was site-specifically labeled with these thiol-reactive fluorophores. The Acrylodan results show that the Httex1 binds in a similar extension to zwitterionic and raft-mimicking lipid vesicles (hydrophobic component). Moreover, the N-terminal Nt17 segment interfaces lipid membranes and the C-terminal PRR remains solvent exposed in the membrane-bound state. Finally, fluorescence anisotropy decays of Atto488 attached to Nt17 or PRR also reveal that these domains experience different dynamics upon membrane-binding. The PRR is highly flexible (as an IDP) and the Nt17 adopts a less flexible state upon binding to anionic lipid membranes.

Introduction

General overview of Huntington's disease

Huntington's disease (HD) is a severe autosomal-dominant progressive neurodegenerative disease [1]. HD is caused by a pathological expansion of the CAG trinucleotide repeat, and consequently it belongs to the group of polyglutamine (polyQ) diseases [1]. In this particular case, the CAG repeat expansions occur in the exon 1 of the *HTT* gene (*IT15* gene) located on the short arm of chromosome 4 (4p16.3) [2]. This disorder is rare, inherited and without available cure [1], [3], with an estimated worldwide-prevalence of 5.5-15 in 100,000 persons [3], [4].

In healthy individuals, the CAG trinucleotide expansion contains less than 35 CAG repeats. In the range of 36 to 39 CAG repeats, the onset of HD only happens at a late stage in life and an individual may not even develop any symptoms during the course of its life [5]. Individuals with a CAG repeat length of 40 or greater develop HD (assuming a normal life span) [5]. The CAG length repeats strongly correlated with the severity and the disease onset. With very large CAG expansions (more than 60), the onset could occur below the age of 20. This is known has juvenile HD and accounts for about 7% of HD cases [6].

The huntingtin (HTT) protein is coded by the *HTT* gene and is found in many of the body's tissues but it's mainly expressed in the brain cortex (the cerebellar cortex, the neocortex, the hippocampal formation, and the striatum), more specifically in the cytoplasm of neurons [7], [8]. HTT is a soluble, mostly cytoplasmic, and a large multidomain protein with a molecular weight of 350

kDa (more than 3000 amino acids) [9]. The first exon of the HTT is usually called by Httex1 and is the most studied part of the HTT protein. This fragment is usually generated either by an aberrant splicing event in which the mRNA transcript originated from *HTT* gene is involved, or by the proteolysis of the full-length HTT. Httex1 is comprised by three major domains: the N-terminal 17 amino acid domain (Nt17 segment), the polyQ tract, and finally the C-terminal proline-rich domain (PRR). All of these domains are highly disordered in solution and are able to modulate the misfolding, oligomerization and fibrillation of both Httex1 and the full-length protein [10]. The Nt17 domain is characterized for being composed of 17 amino acids, mostly conserved between vertebrates, and by forming an amphipathic α-helix that interacts with lipid membranes [11], [12]. The Nt17 domain functions as a cytoplasmic retention signal and is subject to several post-translational modifications (PTMs) [13]. Following this domain, the polyglutamine (polyQ) stretch contains the sequence of the CAG trinucleotide repetitions, whose length in mHTT is highly related to the severity and the HD onset. The proline-rich region (PRR) follows the polyQ domain and is only present in mammals, suggesting that is very recent in terms of evolution of the HTT protein [14]. Even though this domain seems to be important for mediating protein-protein interactions (since it is critical for interactions with proteins that contain tryptophan or SH3 domains [15]), it is highly variable between individuals and its deletion had no severe effect on mouses [11], [16]. In the C-terminal location of HTT, a nuclear export signal has also been identified [13].

In the mutant form, mHTT is thought to be toxic due to a gain-of-function mutation, which confers to it an enhanced probability of the protein to aggregate, the mHTT is more prone to cleavage and to aberrant splicing, that creates shorter fragments that can aggregate and form inclusion bodies in the cytoplasm, interfering with the normal cellular function. In brains, N-terminal fragments of mHTT has been found post-mortem, suggesting that this region is a key step in the development of HD [17]–[19].

The expanded polyQ domain is responsible for the formation and the deposition of intranuclear and cytoplasmic inclusion bodies formed by fibrillar HTT aggregates. Recent studies have demonstrated that the inclusion bodies might be either a protective or incidental while the smaller and more diffuse aggregates may represent the toxic entities [11], [20]–[22]. The flaking domains (polyP and Nt17) which are directly adjacent of the polyQ domain are then a potential target for therapeutical strategies that might help neutralize the toxicity of mHTT aggregates. However, more research is needed in order to reach that objective, including research in how the existence of different conformers mediate the pathogenesis in HD and what is the role of different environmental factors on how they affect those conformers. Membrane elasticity directly influences membrane stability and an alteration to this property might lead to dysfunction of the cell and the consequent disease [23]–[25]. Despite HTT having a prominent membrane location, there is still not much knowledge about the relationship of HTT with lipids and their role in HD. The specific aims of this project were (i) to quantify the binding of Httex1-23Q to lipid vesicles with distinct compositions; (ii) to characterize the role of each flanking polyQ region – N-terminal Nt17 and C-terminal pro-line-rich region (PPR) – in the Httex1-lipid interaction.

Materials and methods

Production of single-labeled Httex1-23Q constructs

In the scope of this thesis, several constructs were created: single-labeled Httex1-23Q constructs at position A2C or A82C with Acrylodan or Atto 488 maleimide. The procedures described below for the recombinant expression and purification of Httex1-23Q were applied to all constructs. Only the labeling was adapted according to previous publications [26]–[28].

Expression of the fusion protein His_6-SUMO-Httex1-23Q

BL21(DE3) One Shot® chemically competent *E. coli* were transformed by heat shock [29] with the pET-SUMO-Httex1-23Q plasmid containing a single mutation in the *HTTEX1* (at position A2C or A82C). The cells were plated on LB-Agar plates supplemented with Km (50 µg/mL) and incubated overnight at 37 ºC. An isolated colony was then inoculated in LB-Km medium and left to grow overnight at 37 ºC with 250 rpm shaking. Next morning, 10 mL of the overnight culture was inoculated in a fresh 90 mL LB-Km medium, which was further grown for approximately 4 hours at 37 ºC, 250 rpm. To scale-up the culture, 1 L LB-Km medium was inoculated with the previous culture for obtaining an optical density at 600 nm (OD_{600}) of 0.1. The cells were then grown at 37 ºC, 250 rpm until they reached an OD_{600} of 0.4-0.8. At this stage, the protein expression was induced with 0.6 mM IPTG, and the culture was left incubating overnight at 16 ºC, 180 rpm. The cells were then collected by centrifugation at 8000 rpm for 10 minutes at 4 ºC and resuspended in 60 mL buffer A (50 mM Tris-HCl, pH 8.0, 500 mM NaCl, 15 mM Imidazole) supplemented with 0.1 mM PMSF and 1 tablet of cOmplete Mini EDTA-free Protease Inhibitor Cocktail. Finally, the cells were stored at -80 ºC until the purification steps.

Purification of the tag-free Httex1-23Q

Cells were initially sonicated (Branson Sonifier 250) on ice with 9 cycles of 15 pulses (50% duty cycle and an output of 9) and 5 minutes of rest between cycles. The cell lysate was then cleared by centrifugation at 17,600 x *g* for 1 hour at 4 ºC. The supernatant was collected and filtered with 0.44-µm syringe filters (low protein binding) to remove leftover cell debris.

A first Immobilized Metal Affinity Chromatography (IMAC) was performed to purify the His_6-SUMO-Httex1-23Q mutated fusion protein in an ÄKTA Start System (GE Healthcare). Briefly, the filtrated lysate was loaded into a 5-mL HisTrap FF column previously equilibrated with buffer A and with a flow rate of 1.5 mL/min. Non-specific bound proteins were washed out with 10 column volumes (CV) of buffer A at a flow rate of 5 mL/min. The fusion protein was then eluted with a gradient of 5–100% of buffer B (50 mM Tris-HCl, pH 8.0, 500 mM NaCl, 500 mM Imidazole) at a flow rate of 1.5 mL/min and in 5-mL fractions.

The fractions with the His_6-SUMO-Httex1-23Q mutated fusion protein were joined, concentrated to about 10 mL and the buffer was exchanged to buffer C (50 mM Tris-HCl, pH 8.0, 150 mM NaCl, 15 mM Imidazole) using an Amicon® Ultra-15 with 10 kDa cutoff. To remove the His_6-SUMO tag, the concentrated fraction was incubated with ubiquitin-like-specific protease 1 containing a His_6-tag (His_6-Ulp1) (1:50) and 1 mM DTT at 4 ºC for 3 hours in a rotator.

A second IMAC was then carried out to purify the tag-free HTT-23Q protein from the protease and the His_6-SUMO tag. Here, the sample was loaded into the 5-mL HisTrap FF column equilibrated with buffer C, and the tag-free protein was

eluted in the flow-through at flow rate of 1.5 mL/min and in 2.5 mL fractions.

The fractions containing the tag-free Httex1-23Q mutated protein were buffer exchanged to buffer SEC (50 mM Tris-HCl, pH 8.0, 200 mM NaCl) with 5 mM DTT and finally concentrated to around 500 µL in an Amicon® Ultra-15 with 3 kDa cutoff. Lastly, a Size Exclusion Chromatography (SEC) was performed to final purification using a Superdex 75 10/300 GL column equilibrated with buffer SEC at a flow rate of 0.3 mL/min and fractions of 0.5 mL were collected.

Labeling of Httex1-23Q-A2C or A82C with Acrylodan or Atto 488 maleimide

About 500–800 µL of freshly purified Httex1-23Q protein with a mutation at position A2C or A82C (concentrations higher than 100 µM) was initially incubated with 1 mM of DTT for 30 minutes at room temperature (RT). The protein was then loaded into two coupled 5 mL-HiTrap desalting columns previously equilibrated with the labeling buffer (20 mM Tris, pH 7.4, 50 mM NaCl, 6 M guanidine hydrochloride). Fractions of 0.5 mL were collected and analyzed by SDS-PAGE.

The protein was then incubated with the fluorescent probe (at a ratio of protein:dye of 1:10): (i) Acrylodan for 4 hours at RT and (ii) Atto 488 maleimide overnight at 4 ºC, both under continued stirring on an amber glass vial protected from light. To purify the labeled Httex1-23Q protein from the free dye, the sample was loaded into the desalting columns now equilibrated with the buffer SEC. Fractions of 0.5 mL were again collected and analyzed by SDS-PAGE.

The fractions containing the protein were further analyzed to determine: (i) the dye concentration by measuring absorbance at 360 nm for Acrylodan ($\varepsilon_{Acrylodan}$ = 12,900 M^{-1} cm^{-1} in water) [30] or at 500 nm for Atto 488 maleimide ($\varepsilon_{Atto\ 488}$ = 90,000 M^{-1} cm^{-1} in Phosphate Buffered Saline, pH 7.4) [31]; and (ii) the protein concentration. We used the Modified Lowry Protein Assay Kit [32], or the BCA Protein Assay Kit [33] for protein quantification with similar results. The protein was then aliquoted in 20 µL fractions, flash-frozen in liquid nitrogen and finally stored at -80 ºC until further use.

Preparation of large unilamellar vesicles

In this work, large unilamellar vesicles (LUVs) of distinct lipid compositions were prepared: (i) pure POPC; (ii) 25:75 POPC:POPS; and (iii) a 1:1:1 SM:Chol:POPC ternary mixture for mimicking lipid rafts [34]. Briefly, the lipid mixtures were extruded through a 50-nm pore diameter polycarbonate membrane in an Avanti Mini-Extruder system to produce LUVs. This procedure was performed at a temperature above the melting temperature of the lipid mixtures. The vesicle diameter and the polydispersity index were confirmed by Dynamic Light Scattering.

Fluorescence spectroscopy

Steady-state fluorescence measurements

Steady-state fluorescence experiments were performed in a Horiba Jobin Yvon Fluorolog 3-22 spectrofluorometer using double monochromators in the excitation/emission and in right angle geometry. The measurements were conducted in 5 x 5 mm quartz cuvettes (Helma Analytics) at RT.

Samples were prepared with a constant protein concentration of 0.6 µM or 50 nM when the fluorescent probe was Acrylodan or Atto 488, respectively, and a variable lipid concentration, ranging from 0 to 1 mM of LUVs. The dilutions to obtain the final concentration of protein were done with a buffer containing 50 mM HEPES, pH 7.4, 50 mM NaCl which was also the buffer used as a blank. The lipid-protein mixtures were prepared on the

day of the fluorescent measurements. The emission spectra were recorded with excitation at 370 nm and 480 nm, for the Httex1-23Q constructs labeled with Acrylodan and Atto 488, respectively. The fluorescence spectral center-of-mass, $\langle\lambda\rangle$, was calculated from the emission spectra, as [35]:

$$\langle\lambda\rangle = \frac{\sum_i I_i \cdot \lambda_i}{\sum_i I_i} \quad (1)$$

where I_i is the fluorescence intensity recorded at the corresponding wavelength λ_i.

For the steady-state fluorescence anisotropy experiments, samples were excited as described before and the polarized emission was detected at the maximum emission wavelength in solution and for the membrane-bound state: (i) for Httex1-23Q labeled with Atto 488 (for both A2C and A82C) was fixed at 520 nm; (ii) for Httex1-23Q-A82C-Acrylodan was recorded exclusively at 525 nm; and finally (iii) for Httex1-23Q-A2C-Acrylodan was detected at 525 nm for solution and at 495 nm for samples with lipid. The fluorescence anisotropy, $\langle r\rangle$, was calculated as:

$$\langle r\rangle = \frac{I_{VV} - G \cdot I_{VH}}{I_{VV} + 2 \cdot G \cdot I_{VH}} \quad (2)$$

with I_{VV} and I_{VH} being the vertical and horizontal components of the polarized fluorescence emission, when the sample is excited with a vertical polarized light, respectively. The G factor is given by the I_{HV}/I_{HH} ratio (which are the components with horizontal excitation) and allows correction for the transmission efficiency of the monochromator to the polarization light. Blanks were always prepared (buffer and lipid), and their data were subtracted to the respective sample. For anisotropy, at least five measurements for each sample were performed, and the data are displayed as a mean with the respective standard deviation.

Time-resolved fluorescence measurements

Time-resolved fluorescence intensity and anisotropy experiments were performed by the time-correlated single-photon timing technique using a step-up previously described [36]–[38]. The setup holds a Jobin-Yvon HR320 monochromator with a cutoff filter and a Hamamatsu R-2809U microchannel plate photomultiplier. Here, we measured the samples previously characterized by steady-state fluorescence (section 0). The Httex1-23Q labeled with Acrylodan was excited at 340 nm (with a frequency doubled secondary cavity-dumped dye laser of DCM-Coherent 701-2) and labeled with Atto 488 at 480 nm (with a BDS-SM-488FBE pulsed picosecond diode laser from Backer & Hickl). The emission was recorded as described above for steady-state fluorescence anisotropy. The fluorescence intensity decays ($I(t)$) were acquired placing the emission polarizer at the magic angle (54.7º) relative to the vertically polarized excitation beam. For the fluorescence anisotropy decays, the parallel (I_{VV}) and perpendicular (I_{VH}) emission polarized components of the fluorescence were alternatively collected. The instrument response function (IRF) was recorded as excitation light scattered by a Ludox solution (silica, colloidal water solution, Aldrich). Fluorescence intensity decays were acquired in 1024 channels.

Fluorescence decay analysis were carried out in TRFA Data Processing Package version 1.4 (developed by the Department of System Analysis and Computer Modelling from Belarusian State University). The goodness of the fits was evaluated from the χ^2 value (<1.4) and a random distribution of weighted residuals and autocorrelation plots.

The florescence intensity decays were analyzed assuming a sum of discrete exponential terms [39]:

$$I(t) = \sum_{i=1}^{n} \alpha_i \exp\left(-\frac{t}{\tau_i}\right) \quad (3)$$

in which α_i and τ_i are the amplitude and the lifetime of the *i*th decay component of fluorescence, respectively [36], [39].

The fluorescence anisotropy decays, $r(t)$, were analyzed by global fitting, where $r(t)$ is described by a sum of discrete exponential terms [38], [39]:

$$r(t) = \sum_{i=1}^{n} \beta_i \exp\left(-\frac{t}{\phi_i}\right) \quad (4)$$

here, β_i and ϕ_i represent the normalized amplitude and the rotational correlation time of the *i*th anisotropy decay component, respectively [36], [39].

Results and discussion

Production of single-labeled Httex1-23Q constructs

The Httex1-23Q production was previously optimized in the host lab. Briefly, Httex1-23Q was expressed in *E. coli* BL21 (DE3) as a fusion protein – containing a His_6-SUMO tag at the N-terminal – at 16 ºC and with 0.6 mM IPTG. Httex1-23Q was engineered to introduce a single-cysteine (position A2C or A82C) for labeling with Acrylodan or Atto 488 maleimide.

The purification of tag-free Httex1-23Q comprised several steps: (1) a first IMAC was performed to purify the mutated His_6-SUMO-Httex1-23Q fusion protein from the cell lysate; (2) the His_6-SUMO tag was cleaved by His_6-Ulp1 protease; (3) a second IMAC was conducted to purify the tag-free Httex1-23Q from the His_6-SUMO tag, the fusion protein and the protease; and finally (4) a SEC was performed for final purification of the tag-free Httex1-23Q. We obtained similar results for the different Httex1-23Q constructs and highly pure protein.

The labeling with the fluorescent probes also occurred as expected. The labeled protein was analyzed by SDS-PAGE and UV-Vis. The dye was quantified by absorbance and using the respective extinction coefficient of each probe. In addition, we used the BCA or Lowry methods for protein quantification, obtaining typical protein concentrations about 15–25 µM (depending on the fraction).

Fluorescence measurements of Httex1-23Q-A2C and -A82C-Acrylodan

This thesis aimed to evaluate the effects of distinct membrane compositions on Httex1-23Q lipid interaction. Initially, we characterized the binding of Httex1-23Q single labeled with Acrylodan at both flanking regions – A2C at N17 and A82C at PRR – with LUVs prepared with variable lipid content. Here, we used Acrylodan, a thiol-reactive probe, to report on local polarity. The Acrylodan fluorescent probe is a thiol reactive probe that forms a very strong and stable bond under the conditions of the fluorescence measurements. This probe is also sensitive to the polarity of the solvent, in both fluorescent intensity and emission wavelength, which are dependent on the effective dielectric constant of the environment that surrounds the probe (solvent) [40]. The bigger the polarity of the solvent, there is a higher solvent relaxation that causes a larger loss of energy, meaning there is a deviation of the spectra to higher wavelengths (red shift). The opposite is also true: if the solvent polarity decreases, there is less solvent relaxation and less loss of energy, and the shift goes to lower wavelengths (blue shift).

Httex1-23Q does not contain any cysteine in its amino acid chains composition. To successfully label the protein with the fluorescent probes, a mutagenesis consisting of a single amino acid substitution was performed, replacing an alanine for a cysteine (that contains a thiol group) in two positions of the primary chain of Httex1-23Q (A2C and A82C), which correspond to the N- (Nt17) and C-

terminal domain of the exon, respectively. The absence of naturally occurring cysteines on the exon allows for a specific labeling on the desired location. The fluorescence properties of Acrylodan coupled to both regions were characterized through steady-state and time-resolved fluorescence measurements.

We used LUVs composed of three different lipid mixtures: pure POPC, 1:1:1 SM:Chol:POPC and 25:75 POPC:POPS. The corresponding parameters obtained from the fluorescence emission spectra, including $\langle\lambda\rangle$ and the normalized integrated area of the respective spectra, are presented in Figure 1. Additionally, in Figure 1 are also displayed the $\langle r\rangle$ and $\langle\tau\rangle$, which is also graphically represented in Figure 2.

Characterization of Httex1-23Q-A2C and -A82C in solution

As previously mentioned, Acrylodan is a highly sensitive fluorescent probe that is affected by the polarity of the surrounding environment. The fluorescent properties of Acrylodan (Figure 1) located at the Nt17 domain (Httex1-23Q-A2C construct) were slightly different from those observed at the PRR (Httex1-23Q-A82C construct). The λ max observed for the A82C-labeled construct in solution is typical of disordered regions as previously reported, where it has been shown to be around 530 nm [41]. Nevertheless, the λ max observed for Httex1-23Q-A2C showed a slight blue-shift from the values of the Httex1-23Q-A82C construct. This is an indication that the Nt17 domain, when in solution, may exhibit transient secondary structures or a more collapsed conformation. It could partially shield the Acrylodan probe from the surrounding solvent (which in this study is mostly water, highly polar) and therefore decrease the local polarity experienced by Acrylodan. This is a plausible explanation for the slight decrease of λ max and the observed differences for the other parameters as well.

Characterization of the Nt17 domain (Httex1-23Q-A2C-Acrylodan) in the presence of lipid vesicles

The Httex1-23Q-A2C-Acrylodan construct was used here to map changes in the local polarity within the Nt17 domain upon membrane interaction. It is expected that when Acrylodan shifts from an environment with high polarity (solution) to a more hydrophobic environment (such as lipid membranes), the maximum emission wavelength will shift towards lower wavelengths. That is often referenced as a blue shift.

The interaction of Httex1-23Q-A2C-Acrylodan with fluid/zwitterionic lipid membranes composed of pure POPC was initially characterized. Upon increasing the lipid concentration, the Acrylodan fluorescence intensity and the mean fluorescence lifetime increased. At 1 mM of POPC LUVs, there are noticeable differences in the fluorescent properties observed for the A2C construct when compared to the solution state (in buffer). The blue-shift (Figure 1(A)) in both λ max and $\langle\lambda\rangle$ indicate that Acrylodan is present in a less polar environment upon adding POPC vesicles. The values are somewhat consistent (at lower extents) to previous findings that showed similar results when a protein labeled with Acrylodan is embedded in a lipid layer [41]. In addition, the increase in the steady-state fluorescence anisotropy suggests that the fluorescent probe (in the A2C position) is more constrained (a lower “freedom of movement”), reporting the membrane-binding.

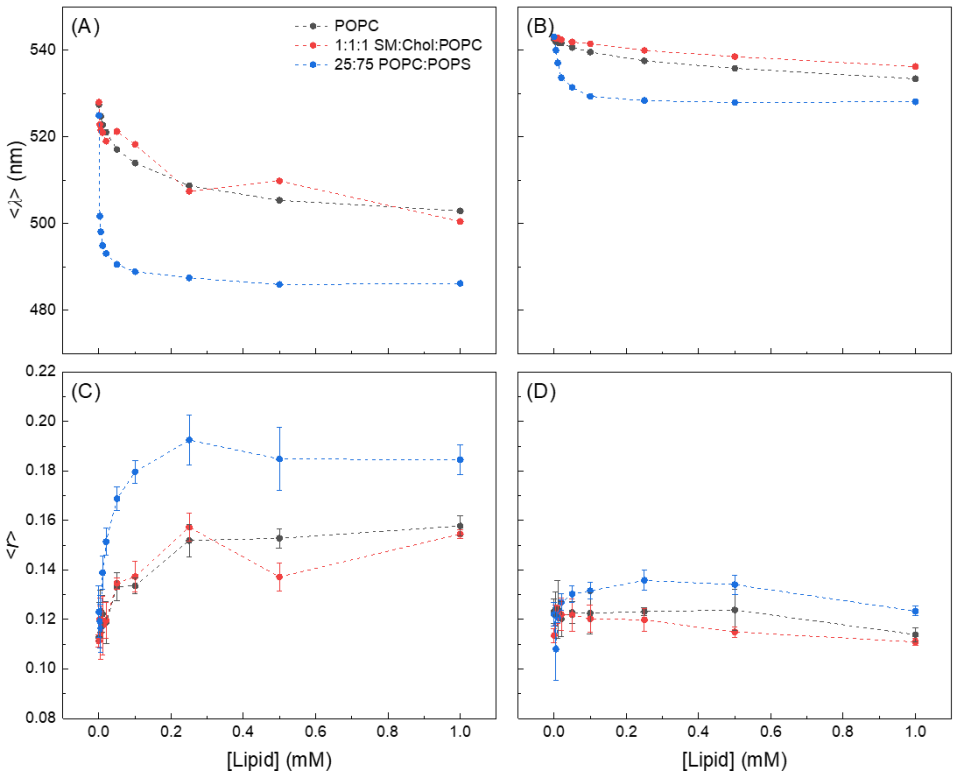

Figure 1 – Fluorescence properties of the (A, C) Httex1-23Q-A2C-Acrylodan and (B, D) Httex1-23Q-A82C-Acrylodan-labeled constructs. Variations of (A-B) $\langle\lambda\rangle$, and (E-F) $\langle r\rangle$ with the lipid concentration. LUVs composed of POPC (black), 1:1:1 SM:Chol:POPC (red) and 25:75 POPC:POPS (blue) were used. The samples had a protein concentration of 0.6 μM and were in a 50 mM HEPES, pH 7.4, 50 mM NaCl buffer at RT. For steady-state fluorescence anisotropy, 10 nm slits in both the excitation and emission were used for Httex1-23Q-A2C-Acrylodan, while for the Httex1-23Q-A82C-Acrylodan was employed 5 nm and 8 nm for the entrance and exit slits, respectively. Characterization of the Nt17 domain (Httex1-23Q-A2C-Acrylodan) in the presence of lipid vesicles

The binding of Httex1-23Q-A2C-Acrylodan with 1:1:1 SM:Chol:POPC LUVs with co-existing of liquid ordered (lo) or disordered (ld) phases was also studied. The results obtained for this ternary lipid mixture were very similar to the ones obtained for pure POPC vesicles. This supports that Nt17 domain also interfaces the lipid vesicles.

The interaction of Httex1-23Q-A2C-Acrylodan with lipid vesicles containing 25:75 POPC:POPS (negatively-charged membranes) was not performed during this work, as the results were previously obtained in the host lab by Dr. Tânia Sousa. However, the properties observed are available for comparison with the other lipid mixtures used in Figure 1 and Figure 2. The results obtained with 25:75 POPC:POPS LUVs show that the Httex1-23Q interaction with anionic lipid membranes was of a greater extent when compared to POPC and 1:1:1 SM:Chol:POPC lipid vesicles.

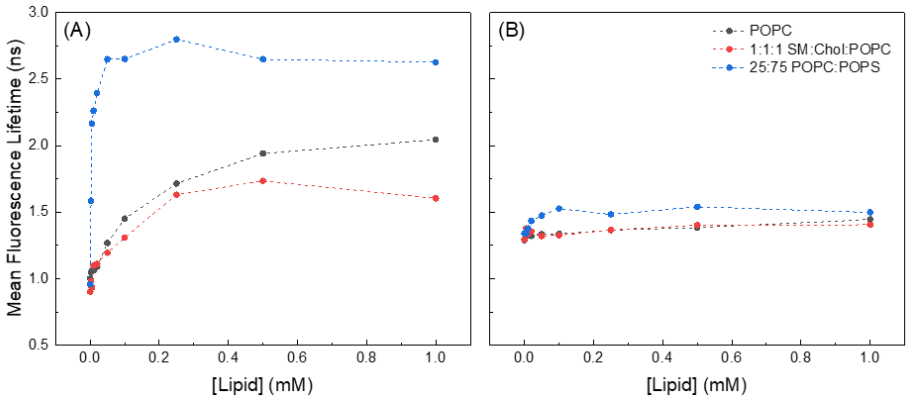

Figure 2 – Changes in the amplitude-weighted mean fluorescence lifetime ($\langle\tau\rangle$) of (A) Httex1-23Q-A2C-Acrylodan and (B) Httex1-23Q-A82C-Acrylodan with increasing lipid concentrations. The measurements were performed with LUVs composed of pure POPC (black); 1:1:1 SM:Chol:POPC (red); and 25:75 POPC:POPS (blue). Dashed lines were drawn as guides to the eye. The samples had a protein concentration of 0.6 µM and were in a 50 mM HEPES, pH 7.4, 50 mM NaCl buffer at RT.

Characterization of the PRR (Httex1-23Q-A82C-Acrylodan) in the presence of lipid vesicles

Previous studies show that the PRR does not adopt a stable secondary/tertiary structure and it is an IDP in solution [42]. In this work, the Httex1-23Q-A82C construct was used to investigate the PRR region's behavior under different lipid mixtures and concentrations (Figure 1 and Figure 2).

Upon increasing the lipid concentration and for all three lipid mixtures, the magnitude of changes in the fluorescence properties of Httex1-23Q-A82C-Acrylodan were significantly smaller than the obtained for the Httex1-23Q-A2C-Acrylodan. There was only a very slight blue-shift in $\langle\lambda\rangle$ and λ max (even for LUVs containing 25:75 POPC:POPS lipid mixture). Moreover, both the steady-state anisotropy and the mean fluorescence lifetime remained practically unchanged.

Altogether, these results show that PRR remains exposed to the solvent Httex1-23Q is in the membrane-bound state, and in contrast the Nt17 domain is directly involved in the membrane-binding of Httex1-23Q.

Time-resolved fluorescence anisotropy measurement of Httex1-23Q-A2C and -A82C-Atto488

The results obtained from the anisotropy decays analysis of both Httex1-23Q-A2C and -A82C-Atto488 constructs are summarized in Table 1. In solution (buffer), the anisotropy decays of both Httex1-23Q-A2C-Atto488 and -A82C-Atto488 were similar and they are characterized by a high β_1 amplitude (for ϕ_1), reflecting a high contribution of the fast rotation of the fluorophore (Atto488) that is typical of IDPs. In the presence of lipid membranes, the anisotropy decays of Httex1-23Q-A2C-Atto488 only experienced major changes upon interaction with anionic vesicles (25:75 POPC:POPS). Specifically, the second rotational correlation time increased for ϕ_2 = 7.96, reflecting that the Nt17 (A2C-postion) interfaces the lipid membranes and adopts a less flexible state. For the Httex1-23Q-A82C-Atto488, we didn´t detect significant variations in the anisotropy decays upon adding 1mM LUVs and for all lipid compositions. This is consistent with our Acrylodan data that the PRR of Httex1 is not involved in the membrane interaction, remining highly flexible/dynamic in the membrane-bound state.

Overall, these data show that N17 adopts a less flexible state upon binding to negatively-charged membranes. The PRR remains highly dynamic even upon membrane binding (independently of the lipid composition).

Table 1 – Time-resolved fluorescence anisotropy parameters of Httex1-23Q-A2C-Atto488 and Httex1-23Q-A82C-Atto488 in buffer (solution) and with 1 mM LUVs (POPC, 1:1:1 SM:Chol:POPC and 25:75 POPC:POPS). β_i is the normalized amplitudes and ϕ_i is the rotational correlation times. $\langle r \rangle_{exp}$) is the steady-state fluorescence anisotropy; and finally $\langle r \rangle_{calc}$ is the anisotropy calculated from the parameters of the time-resolved analyses.

Construct	Solution	$r(0)$	β_1	ϕ_1 (ns)	β_2	ϕ_2 (ns)	χ^2	$\langle r \rangle_{exp}$	$\langle r \rangle_{calc}$
Httex1-23Q-A2C	Buffer	0.335	0.235	0.335	0.100	2.506	1.123	0.074	0.069
	POPC	0.395	0.225	0.185	0.170	1.275	1.274	0.076	0.069
	1:1:1 SM:Chol:POPC	0.394	0.277	0.248	0.117	3.022	1.458	0.077	0.080
	75 mol% POPS	0.403	0.299	0.331	0.104	7.964	1.252	0.103	0.090
Httex1-23Q-A82C	Buffer	0.390	0.242	0.175	0.148	1.688	1.185	0.057	0.052
	POPC	0.397	0.241	0.208	0.156	1.271	1.402	0.064	0.059
	1:1:1 SM:Chol:POPC	0.396	0.240	0.197	0.156	1.471	1.551	0.067	0.064
	75 mol% POPS	0.388	0.218	0.176	0.170	0.887	1.205	0.056	0.056

Conclusion and final remarks

The results shows that Httex1-23Q-A2C-Acrylodan binds to LUVs composed of SM:Chol:POPC and pure POPC vesicles, revealing there is a hydrophobic component in this interaction and no preference for ordered phase. However, this interaction was lower than for POPS-containing vesicles (data obtained previously by Dr. Tânia Sousa). Moreover, the data obtained for Httex1-23Q-A82C-Acrylodan indicate that the C-terminal PRR is completely solvent exposed in the Httex1-23Q membrane-bound state. At second phase, the conformational dynamics of both Nt17 and PRR upon membrane binding was evaluated through time-resolved fluorescence anisotropy measurements. Altogether, these data reveal that Nt17 interfaces POPS-containing vesicles and adopts a less flexible state. While PRR keep its solution conformational dynamics (for all distinct lipid compositions).

Acknowledgement: This document was written and made publicly available as an institutional academic requirement and as a part of the evaluation of the MSc thesis in Biotechnology of the author at Instituto Superior Técnico. The work described herein was performed at the Institute for Bioengineering and Biosciences of Instituto superior Técnico (Lisbon, Portugal), during the period March – September 2022, under the supervision of Dr. Ana Melo and Prof. Ana Azevedo.

References

[1] S. N. Illarioshkin, S. A. Klyushnikov, V. A. Vigont, Yu. A. Seliverstov, and E. V. Kaznacheyeva, 'Molecular Pathogenesis in Huntington's Disease', *Biochem. Mosc.*, vol. 83, no. 9, pp. 1030–1039, Sep. 2018.

[2] M. E. MacDonald *et al.*, 'A novel gene containing a trinucleotide repeat that is expanded and unstable on Huntington's disease chromosomes', *Cell*, vol. 72, no. 6, pp. 971–983, Mar. 1993.

[3] S. S. Baig, M. Strong, and O. W. Quarrell, 'The global prevalence of Huntington's disease: a systematic review and discussion', *Neurodegener. Dis. Manag.*, vol. 6, no. 4, pp. 331–343, Aug. 2016.

[4] P. Dayalu and R. L. Albin, 'Huntington Disease', *Neurol. Clin.*, vol. 33, no. 1, pp. 101–114, Feb. 2015.

[5] Nicholas S Caron, G. E. Wright, and M. R. Hayden, ‘Huntington Disease’, *Huntingt. Dis.*, p. 34.
[6] F. Squitieri, L. Frati, A. Ciarmiello, S. Lastoria, and O. Quarrell, ‘Juvenile Huntington’s disease: Does a dosage-effect pathogenic mechanism differ from the classical adult disease?’, *Mech. Ageing Dev.*, vol. 127, no. 2, pp. 208–212, Feb. 2006.
[7] PubChem, ‘HTT - huntingtin (human)’. https://pubchem.ncbi.nlm.nih.gov/gene/HTT/human (accessed Feb. 02, 2022).
[8] J. A. Sayer, M. Manczak, L. Akileswaran, P. H. Reddy, and V. M. Coghlan, ‘Interaction of the nuclear matrix protein NAKAP with HypA and huntingtin’, *NeuroMolecular Med.*, vol. 7, no. 4, pp. 297–310, Nov. 2005.
[9] G. Bates, P. S. Harper, and L. Jones, Eds., *Huntington’s disease*, 3rd ed. in Oxford monographs on medical genetics, no. no. 45. Oxford ; New York: Oxford University Press, 2002.
[10] Q. Guo *et al.*, ‘The cryo-electron microscopy structure of huntingtin’, *Nature*, vol. 555, no. 7694, pp. 117–120, Mar. 2018.
[11] F. Saudou and S. Humbert, ‘The Biology of Huntingtin’, *Neuron*, vol. 89, no. 5, pp. 910–926, Mar. 2016.
[12] R. S. Atwal, J. Xia, D. Pinchev, J. Taylor, R. M. Epand, and R. Truant, ‘Huntingtin has a membrane association signal that can modulate huntingtin aggregation, nuclear entry and toxicity’, *Hum. Mol. Genet.*, vol. 16, no. 21, pp. 2600–2615, Nov. 2007.
[13] M. P. Parsons and L. A. Raymond, ‘Chapter 20 - Huntington Disease’, in *Neurobiology of Brain Disorders*, M. J. Zigmond, L. P. Rowland, and J. T. Coyle, Eds., San Diego: Academic Press, 2015, pp. 303–320.
[14] M. Tartari *et al.*, ‘Phylogenetic Comparison of Huntingtin Homologues Reveals the Appearance of a Primitive polyQ in Sea Urchin’, *Mol. Biol. Evol.*, vol. 25, no. 2, pp. 330–338, fevereiro 2008.
[15] P. Harjes and E. E. Wanker, ‘The hunt for huntingtin function: interaction partners tell many different stories’, *Trends Biochem. Sci.*, vol. 28, no. 8, pp. 425–433, Aug. 2003.
[16] M. Neveklovska, E. B. D. Clabough, J. S. Steffan, and S. O. Zeitlin, ‘Deletion of the Huntingtin Proline-Rich Region does not Significantly Affect Normal Huntingtin Function in Mice’, *J. Huntingt. Dis.*, vol. 1, no. 1, pp. 71–87, Jan. 2012.
[17] J. M. M. B. dos Santos, ‘The Role of Post-Translational Modifications on the Oligomerization, Aggregation and Toxicity of Mutant Huntingtin’, PhD Thesis, Faculdade de Medicina da Universidade Lisboa, 2018.
[18] Y. J. Kim *et al.*, ‘Caspase 3-cleaved N-terminal fragments of wild-type and mutant huntingtin are present in normal and Huntington’s disease brains, associate with membranes, and undergo calpain-dependent proteolysis’, *Proc. Natl. Acad. Sci. U. S. A.*, vol. 98, no. 22, pp. 12784–12789, Oct. 2001.
[19] A. Lunkes *et al.*, ‘Proteases acting on mutant huntingtin generate cleaved products that differentially build up cytoplasmic and nuclear inclusions’, *Mol. Cell*, vol. 10, no. 2, pp. 259–269, Aug. 2002.
[20] K. A. Burke, K. M. Hensal, C. S. Umbaugh, M. Chaibva, and J. Legleiter, ‘Huntingtin disrupts lipid bilayers in a polyQ-length dependent manner’, *Biochim. Biophys. Acta BBA - Biomembr.*, vol. 1828, no. 8, pp. 1953–1961, Aug. 2013.
[21] M. Arrasate, S. Mitra, E. S. Schweitzer, M. R. Segal, and S. Finkbeiner, ‘Inclusion body formation reduces levels of mutant huntingtin and the risk of neuronal death’, *Nature*, vol. 431, no. 7010, pp. 805–810, Oct. 2004.
[22] P. J. Muchowski, ‘Protein misfolding, amyloid formation, and neurodegeneration: a critical role for molecular chaperones?’, *Neuron*, vol. 35, no. 1, pp. 9–12, Jul. 2002.
[23] K. A. Burke, K. J. Kauffman, C. S. Umbaugh, S. L. Frey, and J. Legleiter, ‘The Interaction of Polyglutamine Peptides with Lipid Membranes Is Regulated by Flanking Sequences Associated with Huntingtin’, *J. Biol. Chem.*, vol. 288, no. 21, pp. 14993–15005, May 2013.
[24] P. A. Janmey and D. A. Weitz, ‘Dealing with mechanics: mechanisms of force transduction in cells’, *Trends Biochem. Sci.*, vol. 29, no. 7, pp. 364–370, Jul. 2004.
[25] V. Vogel and M. Sheetz, ‘Local force and geometry sensing regulate cell functions’, *Nat. Rev. Mol. Cell Biol.*, vol. 7, no. 4, Art. no. 4, Apr. 2006.
[26] X.-H. Li, J. A. Culver, and E. Rhoades, ‘Tau Binds to Multiple Tubulin Dimers with Helical Structure’, *J. Am. Chem. Soc.*, vol. 137, no. 29, pp. 9218–9221, Jul. 2015.
[27] A. M. Melo, S. Elbaum-Garfinkle, and E. Rhoades, ‘Insights into tau function and dysfunction through single-molecule fluorescence’, *Methods Cell Biol.*, vol. 141, pp. 27–44, 2017.
[28] A. M. Melo, J. Coraor, G. Alpha-Cobb, S. Elbaum-Garfinkle, A. Nath, and E. Rhoades, ‘A functional role for intrinsic disorder in the tau-tubulin complex’, *Proc. Natl. Acad. Sci. U. S. A.*, vol. 113, no. 50, pp. 14336–14341, Dec. 2016.
[29] A. Froger and J. E. Hall, ‘Transformation of plasmid DNA into *E. coli* using the heat shock method’, *J. Vis. Exp. JoVE*, no. 6, p. 253, 2007.

[30] F. G. Prendergast, M. Meyer, G. L. Carlson, S. Iida, and J. D. Potter, 'Synthesis, spectral properties, and use of 6-acryloyl-2-dimethylaminonaphthalene (Acrylodan). A thiol-selective, polarity-sensitive fluorescent probe', *J. Biol. Chem.*, vol. 258, no. 12, pp. 7541–7544, Jun. 1983.
[31] 'ATTO 488', *ATTO-TEC GmbH*. https://www.atto-tec.com/ATTO-488.html?language=en (accessed Oct. 05, 2022).
[32] 'Pierce™ Modified Lowry Protein Assay Kit'. https://www.thermofisher.com/order/catalog/product/23240 (accessed Feb. 03, 2022).
[33] 'Pierce™ BCA Protein Assay Kit'. https://www.thermofisher.com/order/catalog/product/23225 (accessed Sep. 05, 2022).
[34] R. F. M. de Almeida, A. Fedorov, and M. Prieto, 'Sphingomyelin/Phosphatidylcholine/Cholesterol Phase Diagram: Boundaries and Composition of Lipid Rafts', *Biophys. J.*, vol. 85, no. 4, pp. 2406–2416, Oct. 2003.
[35] D. H. J. Lopes, A. Chapeaurouge, G. A. Manderson, J. S. Johansson, and S. T. Ferreira, 'Redesigning the folding energetics of a model three-helix bundle protein by site-directed mutagenesis', *J. Biol. Chem.*, vol. 279, no. 12, pp. 10991–10996, Mar. 2004.
[36] G. Scanavachi, A. Coutinho, A. A. Fedorov, M. Prieto, A. M. Melo, and R. Itri, 'Lipid Hydroperoxide Compromises the Membrane Structure Organization and Softens Bending Rigidity', *Langmuir*, vol. 37, no. 33, pp. 9952–9963, Aug. 2021.
[37] A. M. Melo, J. C. Ricardo, A. Fedorov, M. Prieto, and A. Coutinho, 'Fluorescence Detection of Lipid-Induced Oligomeric Intermediates Involved in Lysozyme "Amyloid-Like" Fiber Formation Driven by Anionic Membranes', *J. Phys. Chem. B*, vol. 117, no. 10, pp. 2906–2917, Mar. 2013.
[38] A. M. Melo, A. Fedorov, M. Prieto, and A. Coutinho, 'Exploring homo-FRET to quantify the oligomer stoichiometry of membrane-bound proteins involved in a cooperative partition equilibrium', *Phys. Chem. Chem. Phys.*, vol. 16, no. 34, pp. 18105–18117, Aug. 2014.
[39] J. R. Lakowicz, *Principles of fluorescence spectroscopy*, 3rd ed. New York: Springer, 2006.
[40] R. E. Hibbs, T. T. Talley, and P. Taylor, 'Acrylodan-conjugated Cysteine Side Chains Reveal Conformational State and Ligand Site Locations of the Acetylcholine-binding Protein', *J. Biol. Chem.*, vol. 279, no. 27, pp. 28483–28491, Jul. 2004.
[41] R. Krishnan and S. L. Lindquist, 'Structural insights into a yeast prion illuminate nucleation and strain diversity', *Nature*, vol. 435, no. 7043, pp. 765–772, Jun. 2005.
[42] J. B. Warner, K. M. Ruff, P. S. Tan, E. A. Lemke, R. V. Pappu, and H. A. Lashuel, 'Monomeric Huntingtin Exon 1 Has Similar Overall Structural Features for Wild-Type and Pathological Polyglutamine Lengths', *J. Am. Chem. Soc.*, vol. 139, no. 41, pp. 14456–14469, Oct. 2017.